Multiple-Regression method for Online Fault Detection and Diagnosis of PV Systems Using Kalman Filter Algorithm

Yehya AL-Rifai
Estia Institute of Technology
University of Bordeaux
64210 Bidart- France
y.alrifai@estia.fr

Adriana Aguilera-Gonzalez
Estia Institute of Technology
64210 Bidart- France
a.aguilera-gonzalez@estia.fr

Ionel Vechiu
Estia Institute of Technology
64210 Bidart- France
i.vechiu@estia.fr

Abstract— **Faults on photovoltaic (PV) systems can drastically degrade Microgrids reliability, and stability, if not promptly detected. Thus, a novel Fault Detection and Diagnosis (FDD) methodology is proposed for online monitoring of PV system DC side. This method is based on multiple non-linear regression to emulate the PV behavior at different weather conditions precisely. The regression method is formulated on the relationship of PV characteristics at the maximum operating point without irradiation sensors. Then, to restrain uncertainties and measurement noises, a Kalman Filter algorithm is used. In addition, an adaptive threshold based on non-linear polynomial regression is developed to detect early fault signature in a PV system. To evaluate the performance of the proposed FDD approach, short circuit fault is investigated via MATLAB/Simulink® at various weather conditions. The result reveals the effectiveness of the proposed FDD method to detect soft faults even at low irradiation.**

Keywords— *PV systems, fault detection and diagnosis, Kalman filter, multiple non-linear regression, soft faults, multi-surface.*

I. INTRODUCTION

Renewable Energy, such as photovoltaic (PV) systems, is a key contributor toward a carbon-free future generation power grid. According to the International Renewable Energy Agency (IRENA), the global cumulative PV capacity integrated into Microgrids (MGs) has grown exponentially [1], with massive expectations rising in the wake of current global energy crisis. However, the proliferation of PV systems into MGs rises new challenges concerning dependability and stability under all circumstances [2]. Although, PV system encounter a variety of physical faults due to the long outdoor exposure. Faults can take place on different PV sides (DC/AC side), where Short Circuit (SC) at DC side, according to PV risk analysis [3], represents the most common electrical faults with the highest severity degree. Consequently, faults in PV system can drastically destabilize MGs or even turn into catastrophic failures, resulting in cascading outages phenomenon [4]. Therefore, a real-time Fault Detection and Diagnosis (FDD) strategy is critical to detect and identify early fault signature in PV systems. FDD strategy enhance MG stability and security by allowing its controller to take the appropriate accommodating and mitigating action [5]. Thus, FDD scheme is paramount to preserve the MG required performance even under fault occurrence.

As a result, electrical-based FDD methods have gained recently outstanding popularity due to their robustness [6]. These FDD methods can be broadly classified into two main approaches: (1) Current-Voltage ($I - V$) curve analysis, or (2) power losses analysis through power or current and voltage

measurement under global Maximum Power Points (MPP). For instance, to identify abnormal behavior, in [7] a low-cost methodology is developed based on the $I - V$ curve analysis by periodically measuring open circuit voltage and short circuit current. In [8] the $I - V$ curve is used to detect ground fault, SC, and faulty connection by comparing the curve of healthy string to those of the faulty strings. Then, the method is integrated into principal component analysis to classify these faults. However, $I - V$ curve method can only be performed during day/light hours and not able to detect intermittent faults in a PV plant. In addition, it requires special expensive tool.

Alternatively, FDD method based on PV electrical measurement under MPP are more promising. For instance, in [9] fault alarm is triggered if the difference between the simple power-based method and measured MPP power outputs exceed a defined threshold. Although the detection process is simple, the unpredicted changes in irradiation could generate false alarms. In addition, the method could not classify and localize faults. In [10] a cubic polynomial regression method based on the relationship of PV characteristics in combination with KF is used to diagnose output power lowering in a PV array. The diagnosis method is performed at elevated Irradiation (G>600 W/m²) to detect temporary and partial shading. However, this method is not reliable as the single cubic regression cannot describe the high nonlinearity of I_{mpp} and V_{mpp} relationship at lower irradiation. Thereby, this method could generate problematic false alarms at low irradiation. To improve the diagnosis strategy, in [11] we proposed a multi-zone nonlinear polynomial regression to detect soft SC in a PV system even at low irradiation. However, this method is a two-step methodology where the measured MPP voltage and current are projected to the standard temperature (25°C) before extracting the reference diagnosis using the multi-zone polynomial regression. Thus, the estimation error will certainly increase, leading to an inadequate diagnosis strategy.

Toward this end, this research provides a novel FDD method based on electrical measurement under global MPP to detect soft SC faults in PV systems, avoiding the use of irradiation sensors. The method presented is formulated on a statistical data-driven approach based on Multiple nonlinear Polynomial Regression (MPR) to emulate the PV characteristics under various weather conditions accurately. The MPR method directly derives the relationship of electrical measurement at various temperatures levels. In addition, to restrain the uncertainties and measurement noises, the regression method is integrated into a model based

Table 1. PV module parameters.

1SolTech 1STH-350-WH (350W)		
Maximum Power (P_{MPP})	349.59	W
Open Circuit Voltage (V_{oc})	51.5	V
Short-Circuit Curent (I_{sc})	9.4	A
Voltage at P_{MAX} (V_{MPP})	43	V
Current at P_{MAX} (I_{MPP})	8.13	A
Temperature Coefficient of V_{oc} (α)	-0.36	%/°C
Temperature Coefficient of I_{sc} (β)	0.09	%/°C
Configuration	9S-21P	

through Kalman Filter (KF) algorithm for optimal estimation under dynamic changing conditions. Further, an adaptive threshold based on nonlinear polynomial regression in the state of temperature variable is developed to detect early fault signatures in a PV plant even at low irradiation. Finally, the performance of the proposed FDD method is evaluated via MATLAB/Simulink® at various weather conditions.

The remainder of this paper is structured as follow: Section II describes the multiple nonlinear regression method developed in this study. The FDD strategy using KF is presented in Section III, along with the proposed adaptive threshold. The simulation results are discussed in Section IV. Finally, the conclusion and perspectives are given in Section V.

II. MULTIPLE NONLINEAR POLYNOMIAL REGRESSION METHOD

The main purpose is to establish a reliable estimation method to examine the PV status despite the harsh operating conditions. Thus, a statistical regression method is proposed to describe the nonlinear PV behavior at variable irradiation and temperature. The regression method is formulated at global MPP based on the relationship between PV characteristics; current, temperature and voltage ($I_{mpp}, T,$ and V_{mpp}), avoiding the use of irradiation sensors. The statistical relationship is derived from MPR based on multiple independent variables to predict optimally the outcome response variable $V_{ref,diag} = f(I_{MPP}, T)$ at various weather conditions. Therefore, to establish the numerical relationship among variables a dataset, based on the real meteorological profiles [12], is initially generated using the 1-single diode model with additional shunt resistance in parallel [13], as expressed by:

$$I_{pv} = N_p I_{ph} - N_p I_0 \left[e^{\frac{1}{aV_t}\left(\frac{V_{pv}}{N_s} + \frac{I_{pv}R_s}{N_p}\right)} - 1 \right] - \frac{N_p \frac{V_{pv}}{N_s} + I_{pv}R_s}{R_{sh}} \quad (1)$$

where I_{ph} is the photocurrent, a is the ideality factor, I_0 denotes the dark saturation current, V_t is the thermal voltage. The shunt resistance R_{sh} represents the leakage current path caused by the distributed manufacturing defects inside the solar cell. The series resistance R_s stands for the power dissipation caused by the thermal effect in the whole junction substrates and the electrical contacts. N_s and N_P are the number of series and parallel cells in a module, respectively. I_{pv} and V_{pv} depict the terminal current and voltage of the PV

module, respectively. In this paper, Soltech-1STH-350-WH panel is used, and its electrical parameters are presented in **Table 1**. In addition, a maximum power point tracking based on KF technique is employed to harvest the maximum power yield in the PV system [14].

Thereby, the generated datasets via MATLAB/Simulink® are split into training data (660 data for each feature) and test-data (364 data for each feature). Aiming to extract the best-fitting surface and avoid high variance, a loss-function analysis is conducted at different MPR degrees under training/test dataset. The loss-function is based on three evaluation indices as follow:

$$adj - R^2 = (1 - R^2)\frac{(o - 1)}{(o - K - 1)}$$

$$RMSE = \sqrt{\frac{1}{N}\sum_{i=1}^{o}[y(i) - \hat{y}(i)]^2} \quad (2)$$

$$MAPE = \frac{1}{n}\frac{\sum_{i=1}^{o}|y(i) - \hat{y}(i)|}{y(i)}$$

where $y(i)$ is the real measured value, $\hat{y}(i)$ denotes the estimated value of the polynomial, o is the number of samples, $\bar{y}(i)$ represents the mean of real values. The numerical goodness-fit $adj - R^2$ describes how well the predicted variables can explain the variation in the response variable, considering the number of predictors K. In addition, RMSE gives an image of the error magnitude, while MAPE is useful for understanding the relative size of the error.

A rigorous estimation method is critical for reliable diagnosis strategy, allowing to detect soft faults in PV systems while minimizing missing and false alarms even at minor irradiation.

A. Single surface MPR

The relationship between voltage diagnosis indicator ($V_{ref,diag}$) and the independent variables (I_{mpp}, T) can be described by single surface MPR as expressed by Eq.(3).

$$V_{ref,diag} = \sum_{\{i=0\}}^{\{n\}} \sum_{\{j=0\}}^{\{p\}} \beta_{ij} I_{mpp}^i T^j \quad (3)$$

where n and p stands for the polynomial degree of the independent variable I_{mpp} and T, respectively. β_{ij} represents the MPR coefficient. The outcome variable $V_{ref,diag}$ represents the voltage reference diagnosis (estimated by KF). The goodness fit of MPR under training data at different degrees is evaluated in **Fig. 1**. The MPR degrees with coefficients less than 8 are underfitted. Even the 4th degree $V_{ref,diag} = f(I_{mpp}^3, T^1)$ have an RMSE =4.8 V. Whereas, the higher degrees have poor fitting accuracy. The seventh degree $V_{ref,diag} = f(I_{mpp}^4, T^3)$ have an RMSE = 3.5V. Further, the evaluation under the test-dataset, **Fig. 2**, reveals that the single surface MPR are strongly overfitted at minor irradiation. The percentage estimation error is greater than 15% for low degrees, and more than 7% for higher degrees. Consequently, the single surface MPR method are
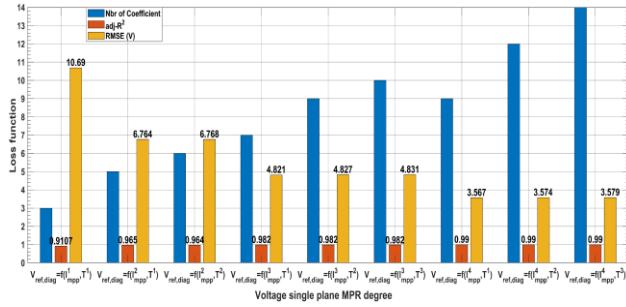
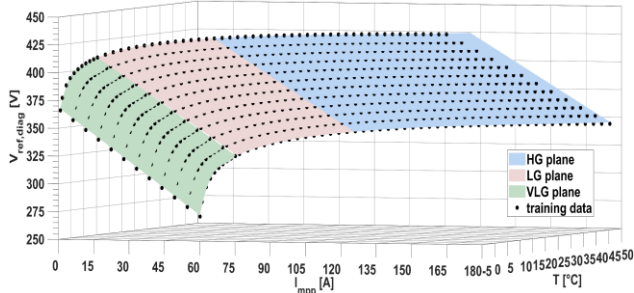**Fig. 1.** Loss function of single surface MPR under training data.

Fig. 2. Percentage error of single surface under test-data.

Fig. 3. Multi-Surface MPR method.
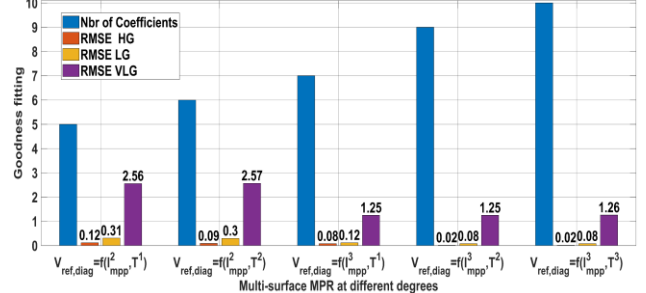
Fig. 4. Loss function multi-surface MPR under training data

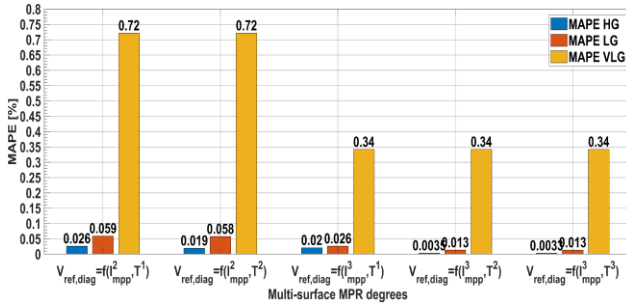**Fig. 5**. MAPE multi-surface MPR under test-data.
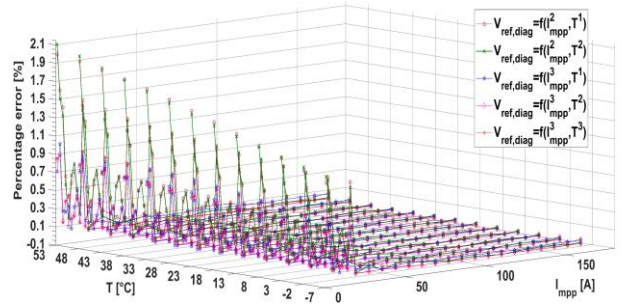
Fig. 6. Percentage error of multi-surface MPR under test-data.

not reliable, resulting in missing and false alarms. Therefore, to describe the relationship of PV characteristics accurately, an improved estimation method is proposed based on the multi-surface MPR.

B. Multi-surface MPR method

Aiming to reduce the estimation error due to the high nonlinearity, a multi-surface according to irradiation level is suggested, as represented in **Fig. 3**. Thus, the relationship is described by three surfaces: The first surface in blue represents the high irradiation (HG) region (where $G \geq 400$ W/m²), the Low irradiation (LG) is represented by the second surface in red (where $100 \leq G < 400$ W/m²), while the Very Low irradiation (VLG) region is represented by the third surface in green (where $G < 100$ W/m²). As this method is irradiation sensor less, hence, the surfaces are split with respect to MPP current which is an irradiation image.

The loss function analysis for the multi-surface MPR method at different degrees under fitting data is evaluated in **Fig. 4**. The estimation errors using multi-surface MPR have significantly dropped in different regions. Notably, the third-degree multi-surface $V_{ref,diag} = f(I_{mpp}^2, T^1)$ is better fitted (RMSE < 2.56 V over all regions) than the seventh-degree single surface MPR (RMSE = 3.6 V). Further, the best fitting surfaces is achieved by the 5ᵗʰ degree $V_{ref,diag} = f(I_{mpp}^3, T^2)$ with a less estimation error at HG and LG regions (RMSE <
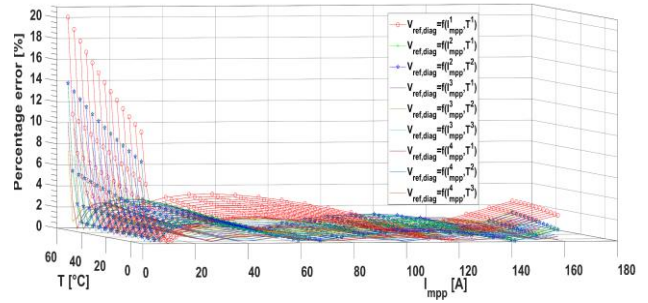
0.08 V). Nevertheless, the 4ᵗʰ degree $V_{ref,diag} = f(I_{mpp}^3, T^1)$ possesses a good estimation performance, and notably outperforms $V_{ref,diag} = f(I_{mpp}^2, T^2)$ at VLG. However, the third surface for different degrees at VLG is relatively more biased. Although, since the voltage variation at VLG is around 12V, the goodness fit is reasonable for high MPR degrees.

To avoid overfitting the different multi-surface MPR degrees are re-assessed under the test-dataset, as shown in **Fig. 5**. The test-dataset unfold that at HG and LG regions even low MPR degrees have low variance. Nevertheless, as the variation of voltage at HG is small (around 0.07V), a robust estimation method is paramount to avoid missing and false alarms. Accordingly, 4ᵗʰ MPR degrees have reasonable estimation accuracy. Although, the fourth degree $V_{ref,diag} = f(I_{mpp}^2, T^2)$ has relatively higher estimation error at VLG (MAPE = 0.72%), where the maximum percentage error exceeds 2%, as shown in **Fig. 6**. However, the 4ᵗʰ-degree $V_{ref,diag} = f(I_{mpp}^3, T^1)$ at VLG is more accurate (MAPE = 0.34 %), with maximum percentage error less than 1%. Further, the higher degrees are better fitted with lower maximum percentage error at VLG region. However, high degrees impose higher computational complexity, affecting the performance of the diagnosis system. Thus, as a trade-off between calculation charge and estimation accuracy, the 4ᵗʰ degree ($V_{ref,diag} = f(I_{mpp}^3, T^1)$) multi-surface is favored
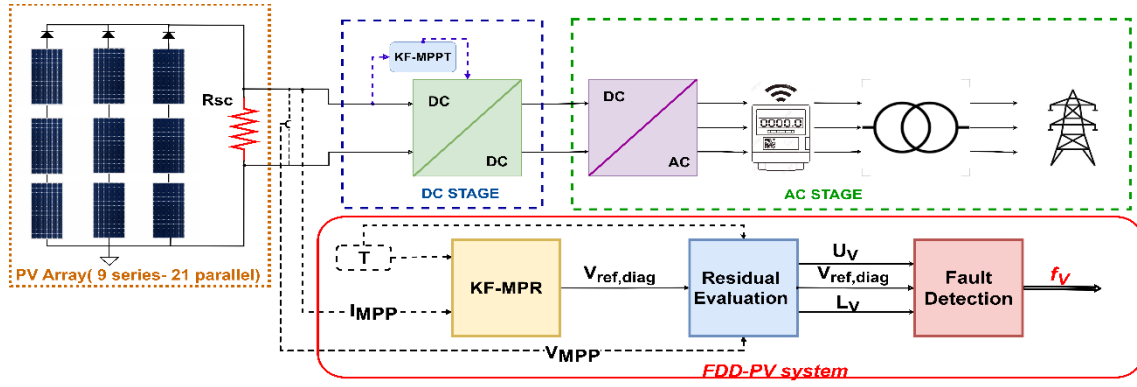
Fig.7. FDD general scheme.

over the three regions. It is worth noting that the same degree is chosen over all surfaces, as the same order impose the same KF structure, avoiding additional complexity. Accordingly, the 4th multi-surface MPR can be formulated as follows:

$$V_{ref,diag}(I_{mpp}, T)$$
$$= \begin{cases} \sum_{\{i=0\}}^{\{3\}} \sum_{\{j=0\}}^{\{1\}} \Psi_{ij} I_{mpp}^i T^j & \forall\, I \geq 68\,A \mid \Psi_{31} = 0 \\ \sum_{\{i=0\}}^{\{3\}} \sum_{\{j=0\}}^{\{1\}} \varphi_{ij} I_{mpp}^i T^j & 17 \leq I < 68\,A \mid \varphi_{31} = 0 \\ \sum_{\{i=0\}}^{\{3\}} \sum_{\{j=0\}}^{\{1\}} \delta_{ij} I_{mpp}^i T^j & I < 17\,A \mid \delta_{31} = 0 \end{cases} \quad (4)$$

where Ψ, φ, δ represents the MPR coefficient at HG, LG, and VLG, respectively. The estimation method proposed in this paper is dependable and able to generalize new dataset at different weather conditions. Consequently, this accurate estimation method will lead to a reliable FDD strategy over all irradiation regions, allowing to detect soft faults while minimizing missing and false alarms.

III. FAULT DETECTION AND DIAGNOSIS METHOD

For a stochastic estimation under noisy measurements, the regression method presented in this research study is integrated into a model-based method through KF algorithm. The structure of the proposed diagnosis algorithm is schematically illustrated in **Fig.7**. The FDD model-based approach consists of two consecutive stages: *residual generation* and *residual evaluation*.

A. Residual generation.

Aiming to adapt the monitoring system to PV dynamic changes and unpredicted situations while handling model uncertainties and measurement noises [15], the MPR method is combined with KF algorithm. This algorithm is employed to estimate optimally the PV reference characteristics (Eq.(4)) to diagnose soft faults in a PV system. The MPR is formulated into a state space representation as follow:

$$x(k+1) = Ax(k) + \omega(k)$$
$$z(k) = Cx(k) + \vartheta(k) \quad (5)$$

where, the state vector $x(k)$ represents the MPR dependent variables from Eq.(4) for voltage diagnosis indicators. A and C are the state and output matrices, respectively. While $z(k)$ denotes the measurement that represents the independent variables I_{mpp}, and T. Finally, ω and ϑ are respectively the process and measurement zero mean Gaussian white noises. The KF equations fall into two-phase process:

1) Time update (prediction state)

Firstly, the recursive algorithm predicts the state using the mathematical model by projecting ahead the current state and error covariance to get a priori estimate for the next time step as follows:

$$\hat{x}_K^- = A\hat{x}_{K-1}$$
$$P_K^- = AP_{K-1}A^T + Q \quad (6)$$

where $\hat{x}^-, P^-$ are the priori state and covariance estimate at iteration (K) from the previous iteration ($K-1$), respectively. Q is the process noise.

2) Measurement update

The priori estimates are then corrected by the Kalman gain (k_k) to obtain the posteriori states as given by Eq.(7).

$$x_K = P_K^- C^T (C\, P_K^-\, C^T + R)^{-1}$$
$$\hat{x}_K = \hat{x}_K^- + k_K(z_k - C\, \hat{x}_K^-)$$
$$P_K = (I - k_K C)P_K^- \quad (7)$$

where $\hat{x}_K$ is the update state. The covariance P_K is a positive definite symmetric matrix with a large initial value $P_0 = diag(4)$ that declares low credibility for initial guess. R is the measurement noise covariance. Indeed, the matrices Q and R are diagonal given more weights to the model.

B. Residual evaluation.

The second stage represents the procedure of decision-making. The PV's status is examined by comparing the analytical predicted value by KF ($V_{ref,diag}$) with the measured V_{mpp}. If the discrepancy exceeds an adaptive threshold, considering the model uncertainties, a fault alarm is triggered. To minimize missing and false alarms, a statistical threshold is formulated on MPR uncertainties in the state of temperature variables. This adaptive threshold is developed on quadratic polynomial regression based on the loss function analyzed in Section II. In addition, the maximum percentage error is significantly lower at elevated
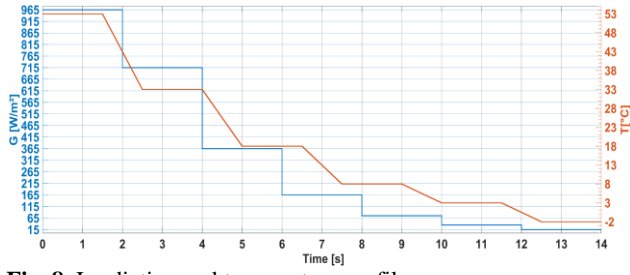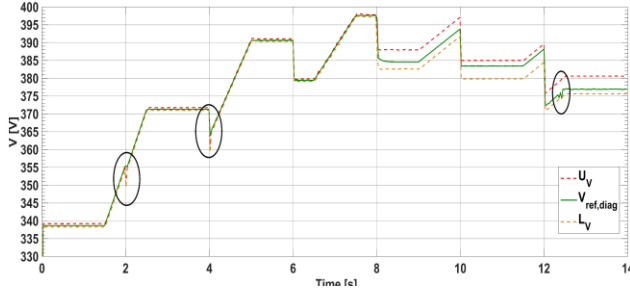
Fig. 8. Irradiation and temperature profile.

Fig. 9. Healthy condition: residual magnitude and fault vector.

Fig.10. Healthy condition: fault diagnosis.
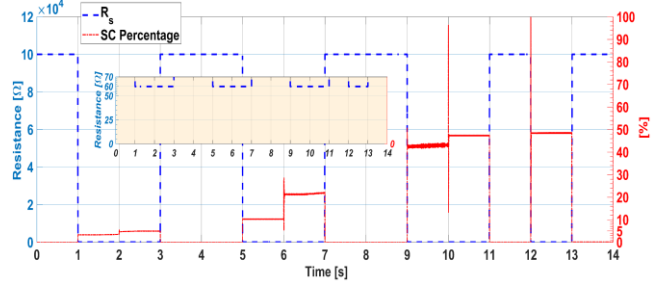
Fig.11. Unhealthy condition: SC magnitude and percentage.
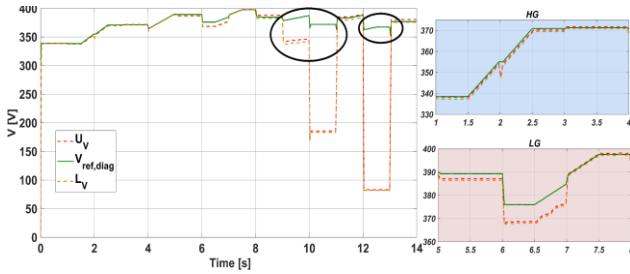

Fig. 12. Unhealthy condition: fault diagnosis
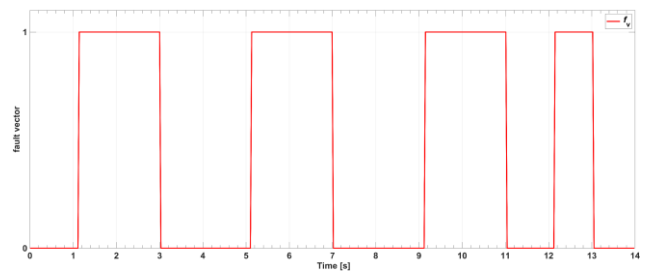
Fig. 13. Unhealthy condition: fault vector.

irradiation comparing with that at VLG. Thus, to keep the threshold closer to the reference diagnosis $V_{ref,diag}$ as possible, the adaptive threshold is divided into two zones and can be formulated as follow:

$$MPE_V(T) = \begin{cases} \sum_{k=0}^{2} \theta_k T^{2-k} & \forall\, I \geq 17\, A \\ \sum_{k=0}^{2} \Lambda_k T^{2-k} & I < 17\, A \end{cases} \quad (8)$$

where T denotes the measured temperature. θ_k and Λ_k represents the polynomial coefficients at elevated irradiation and VLG, respectively. The coefficients are based on the maximum estimation error MPE for voltage diagnosis indicator ($V_{ref,diag}$). Thus, the threshold boundaries are set as follow:

$$\underbrace{(1 - MPE_V)V_{MPP}(k)}_{L_V} < V_{ref,diag}(k)$$
$$< \underbrace{(1 + MPE_V)V_{MPP}(k)}_{U_V} \quad (9)$$

where U_V and L_V stands for the upper and lower threshold. Accordingly, the PV state is examined using a new Boolean fault vector $f_v \in \{0,1\}$ as given in Eq.(10):
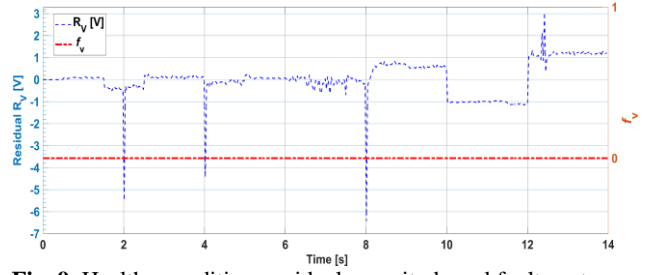
$$f_V = \begin{cases} 1, & if\ V_{ref,diag} > U_V \\ & or\ V_{ref,diag} < L_V \\ \\ 0, & otherwise \end{cases} \quad (10)$$

Thus, if the adaptive threshold gets violated, the fault vector is settled to 1 generating an alarm that indicates the presence of a fault. Otherwise, the fault vector f_v remains 0 denoting a healthy condition.

IV. SIMULATION RESULTS

To evaluate the performance of the proposed FDD methods, two scenarios, *(A) healthy* and *(B) soft SC fault*, are investigated in MATLAB/Simulink®. The irradiation and temperature profile adopted in the simulation is provided in **Fig. 8**. The main idea is to examine the robustness of the proposed FDD method at the different surfaces and extreme temperatures [-2°C; 53°C]. From $t = 0$ sec to $t = 4$ sec the simulation addresses the diagnosis strategy at HG. From $t = 4$ sec to $t = 8$ sec the diagnosis scheme is evaluated at LG. the remaining time is for evaluating the FDD at VLG.

A. Healthy conditions.

In this scenario, a healthy condition is considered to assess the reliability of the proposed FDD scheme at different weather conditions. As shown in **Fig. 9**, The residual (R_V) (i.e., the difference between the measured V_{mpp} and the estimated $V_{ref,diag}$) are very small. At HG and LG, from $t = 0$ sec to $t = 8$ sec, R_V is less than 0.5 V, since the MPR method is perfectly accurate over these two regions.

However, as the maximum percentage error of MPR slightly increases at VLG, the residuals marginally increase to $R_V = 1V$ at VLG. Consequently, it is possible to appreciate in **Fig.10** that despite the harsh operating conditions, the estimated indicator $V_{ref,diag}$ is maintained within the adaptive boundaries. At HG and LG, the adaptive threshold is very close to the reference diagnosis indicators, since the MPR is exactly accurate. Although, from $t = 8$ sec to $t = 14$ sec, the thickness of threshold slightly increases as the maximum percentage error (Eq.(8)) is higher at VLG. However, due to the abrupt drop of irradiation with the decreasing of temperature, the threshold gets violated at $t = 2, 4$, and 8 sec, as highlighted by black circles in **Fig.10**. Thus, to avoid these false alarms, due to MPR's coefficient transition and abrupt weather changing, an alarm delay ($t_d = 0.1$ sec) is added. Thereby, since the threshold is respected, the fault vector f_V in red remains 0, as shown **Fig. 9**, denoting a healthy PV state.

B. Unhealthy conditions: Intermittent SC fault

This scenario investigates the performance of the proposed FDD method for detecting soft SC in a PV system. The fault is configured by adding a soft SC resistance $R_{sc} = 60\,\Omega$ in parallel to PV's string. The fault is intermittently activated at each surface (HG, LG, VLG), as depicted in **Fig.11**. the SC faults is ON from $t = 1$ sec to $t = 3$ sec at HG and from $t = 5$ sec to $t = 7$ sec at LG. Similarly, the soft SC is initiated at VLG from $t = 9$ sec to $t = 11$ sec and from $t = 12$ sec to $t = 13$ sec. Otherwise, the resistance is open circuited. As appreciated, the percentage relative size of SC varies according to irradiation levels. The SC relative size at HG represent around 3% of I_{mpp}, while at LG is less than 20%, and at VLG represents 50%. Remarkably, each time the faults is activated into the PV system the threshold gets violated, as described in **Fig. 12**. The diagnosis indicator $V_{ref,diag}$ exceeds the upper threshold. Accordingly, as depicted in **Fig. 13** a fault alarm is triggered simultaneously, indicating the presence of soft SC with a short mean time to detection delay of 0.14 sec. Therefore, the FDD scheme is able to detect soft SC at harsh operating conditions with short mean time to detection delay.

In comparison to the two-step methodology in [11] which is restricted to unhealthy power dissipation higher than 5%, the FDD scheme is able to detect very soft short circuit ($R_{sc} = 60\,\Omega$) at only 3.5% unhealthy power dissipation.

V. Conclusion

This paper presents a novel FDD scheme to detect soft short circuit in PV systems even at low irradiation levels. The FDD method is formulated on MPR method integrated into KF algorithm for stochastic estimation under noisy measurements. The MPR approach is derived from the relationship between voltage, current and temperature under global MPP, without irradiation sensor. In addition, an adaptive threshold based on quadratic polynomial degree in the state of temperature variable is settled to precisely distinguish between faulty and healthy state. The effectiveness of the proposed FDD scheme is verified by diagnosis results under MATLAB/Simulink®. The FDD scheme can effectively detect intermittent soft SC at an early stage, with a short mean time to detection delay 0.14 sec.

As a future perspective, it is interesting to investigate the robustness of the proposed method against other type of faults, as well integrate fault estimation and isolation to enable the MG's controller to take the appropriate countermeasure action.

References

[1] "Solar energy." https://www.irena.org/Energy-Transition/Technology/Solar-energy (accessed Apr. 16, 2023).

[2] S. Jadidi, H. Badihi, and Y. Zhang, "Design of an intelligent hybrid diagnosis scheme for cyber-physical PV systems at the microgrid level," *International Journal of Electrical Power & Energy Systems*, vol. 150, p. 109062, Aug. 2023, doi: 10.1016/j.ijepes.2023.109062.

[3] M. Herz, G. Friesen, U. Jahn, M. Koentges, S. Lindig, and D. Moser, "Identify, analyse and mitigate—Quantification of technical risks in PV power systems," *Progress in Photovoltaics*, p. pip.3633, Nov. 2022, doi: 10.1002/pip.3633.

[4] S. Jadidi, H. Badihi, and Y. Zhang, "Fault Diagnosis in Microgrids with Integration of Solar Photovoltaic Systems:A Review," *IFAC-PapersOnLine*, vol. 53, no. 2, pp. 12091–12096, 2020, doi: 10.1016/j.ifacol.2020.12.763.

[5] M. Jamali, H. R. Baghaee, M. S. Sadabadi, G. B. Gharehpetian, and A. Anvari-Moghaddam, "Distributed Cooperative Event-Triggered Control of Cyber-Physical AC Microgrids Subject to Denial-of-Service Attacks," *IEEE Trans. Smart Grid*, pp. 1–1, 2023, doi: 10.1109/TSG.2023.3259545.

[6] Y.-Y. Hong and R. A. Pula, "Methods of photovoltaic fault detection and classification: A review," *Energy Reports*, vol. 8, pp. 5898–5929, Nov. 2022, doi: 10.1016/j.egyr.2022.04.043.

[7] A. Y. Jaen-Cuellar, D. A. Elvira-Ortiz, R. A. Osornio-Rios, and J. A. Antonino-Daviu, "Advances in Fault Condition Monitoring for Solar Photovoltaic and Wind Turbine Energy Generation: A Review," *Energies*, vol. 15, no. 15, p. 5404, Jul. 2022, doi: 10.3390/en15155404.

[8] S. Fadhel *et al.*, "PV shading fault detection and classification based on I-V curve using principal component analysis: Application to isolated PV system," *Solar Energy*, vol. 179, pp. 1–10, Feb. 2019, doi: 10.1016/j.solener.2018.12.048.

[9] Y. Stauffer, D. Ferrario, E. Onillon, and A. Hutter, "Power monitoring based photovoltaic installation fault detection," in *2015 International Conference on Renewable Energy Research and Applications (ICRERA)*, Palermo: IEEE, Nov. 2015, pp. 199–202. doi: 10.1109/ICRERA.2015.7418695.

[10] B.-K. Kang, S.-T. Kim, S.-H. Bae, and J.-W. Park, "Diagnosis of Output Power Lowering in a PV Array by Using the Kalman-Filter Algorithm," *IEEE Trans. Energy Convers.*, vol. 27, no. 4, pp. 885–894, Dec. 2012, doi: 10.1109/TEC.2012.2217144.

[11] A.-R. Yehya, A. A. Gonzalez, and I. Vechiu, "Fault Detection and Diagnosis of PV Systems Using Kalman-Filter Algorithm Based on Multi-Zone Polynomial Regression.," presented at the 16th European Workshop on Advanced Control and Diagnosis - ACD2022, Nov. 2022. Accessed: Apr. 17, 2023. [Online]. Available: https://hal.science/hal-03916297

[12] "JRC Photovoltaic Geographical Information System (PVGIS) - European Commission." https://re.jrc.ec.europa.eu/pvg_tools/en/#api_5.2 (accessed Dec. 13, 2022).

[13] A. Jendoubi, F. Tlili, and F. Bacha, "Sliding mode control for a grid connected PV-system using interpolation polynomial MPPT approach," *Mathematics and Computers in Simulation*, vol. 167, pp. 202–218, Jan. 2020, doi: 10.1016/j.matcom.2019.09.007.

[14] B. O. Kang and J. H. Park, "Kalman filter MPPT method for a solar inverter," in *2011 IEEE Power and Energy Conference at Illinois*, Urbana, IL, USA: IEEE, Feb. 2011, pp. 1–5. doi: 10.1109/PECI.2011.5740490.

[15] R. Isermann, *Fault-diagnosis systems: an introduction from fault detection to fault tolerance*. Berlin ; New York: Springer, 2006.